International Journal of Hydrogen Energy 91 (2024) 1080–1092

Contents lists available at ScienceDirect

International Journal of Hydrogen Energy

journal homepage: www.elsevier.com/locate/he

Utilization of fuel synthesis by-products as reducing agents in solar thermochemical syngas production

Philipp Holzemer-Zerhusen [a], Andreas Rosenstiel [a,b,*], Stefan Brendelberger [a], Martin Roeb [a], Christian Sattler [a,b]

[a] Deutsches Zentrum für Luft- und Raumfahrt, Institute of Future Fuels, Linder Höhe, 51147, Köln, Germany
[b] RWTH Aachen University, Faculty of Mechanical Engineering, Chair for Solar Fuel Production, 52062, Aachen, Germany

ARTICLE INFO

Handling Editor: Søren Juhl Andreasen

Keywords:
Ceria
Redox reforming
Solar fuels
Solar syngas
Green hydrogen
Green hydrocarbons
Fischer-tropsch synthesis

ABSTRACT

Solar thermochemical redox cycles followed by a synthesis process are a potentially carbon-neutral way to produce versatile carbonaceous products. The required high temperature of the redox cycle, however is correlated to high heat losses and limits the process efficiency. Use of natural gas as a reductant can lower the temperature, but this approach depends on a fossil carbon source and is not carbon neutral. We propose a novel concept in which short chained hydrocarbons, which are a by-product of the synthesis process are recycled and used as a reductant in the solar redox cycle. In the present study we investigate the use of C_1–C_4 alkanes, which are by-products of high or low temperature Fischer-Tropsch synthesis as reductants in a ceria-based redox cycle. Thermodynamic simulation results imply that both higher degrees of reduction and lower reduction temperatures are feasible and that the energy demand for the reduction step can be decreased by 61% or 24% for high or low temperature Fischer-Tropsch synthesis, respectively.

Symbols

c_p	Molar heat capacity	J mol^{-1} K^{-1}
C	Concentration factor	–
$f_{c,N}$	Fraction of a species with N carbon atoms with respect to the overall number of carbon atoms	–
G	Gibbs free energy	J mol^{-1}
h	Molar enthalpy	J mol^{-1}
$\dot{H}$	Enthalpy flow	W
I_{sol}	Insolation	W m^{-2}
$\dot{n}$	Molar flow rate	mol s^{-1}
N	Number of carbon atoms in a hydrocarbon molecule	–
$\dot{Q}$	Heat flow	W
R	Universal gas constant	J mol^{-1} K^{-1}
δ	Oxygen non-stoichiometry	–
$\Delta_\delta h$	Incremental change of h with respect to δ	J mol^{-1}
σ	Stefan-Boltzmann constant	W m^{-2} K^{-4}
η	Efficiency	–
ν	Stoichiometric factor	–
φ	Recycled fraction of FT product	–
Φ	Vacancy ratio	–
ϕ_i	Fugacity coefficient of component i	–
Subscripts		

(*continued on next column*)

(*continued*)

c	Carbon atom-based quantity
CP	Combustion products
ox	Oxidation
prod	Product
red	Reduction
rec	Receiver
SG	Syngas
Superscripts	
TC	Thermochemical reduction
Th	Thermal reduction
∘	Standard pressure/at standard pressure

1. Introduction

Solar thermochemical redox cycles are a promising pathway towards carbon-neutral fuels and other carbon-based products. Within such processes a redox material is used to split water and/or carbon dioxide to produce hydrogen or syngas, a mixture of hydrogen and carbon monoxide, from solar radiation. A solar syngas can be further processed to a variety of base chemicals or to a liquid fuel *via* well-established synthesis steps like the Fischer-Tropsch (FT) process [1].

Non-stoichiometric ceria is often considered as a reference redox

* Corresponding author. Deutsches Zentrum für Luft- und Raumfahrt, Institute of Future Fuels, Linder Höhe, 51147, Köln, Germany.
E-mail address: Andreas.Rosenstiel@dlr.de (A. Rosenstiel).

https://doi.org/10.1016/j.ijhydene.2024.10.089
Received 12 June 2024; Received in revised form 1 October 2024; Accepted 6 October 2024
Available online 19 October 2024

material for two-step solar thermochemical redox cycles [2,3], due to its fast reaction kinetics [4,5] and high stability [6,7] and was utilized in several experimental campaigns [2,4,8–10]. Still, the thermodynamics of ceria lead to very challenging operation conditions and the search for alternative materials is an ongoing endeavour [11–15]. The water and carbon dioxide splitting process is a two-step thermochemical cycle. The redox material is oxidized by water and/or carbon dioxide forming hydrogen and/or carbon monoxide according to

$$\frac{1}{\Delta\delta}\mathrm{CeO}_{2-\delta_{\mathrm{red}}} + \mathrm{H_2O/CO_2} \rightleftharpoons \frac{1}{\Delta\delta}\mathrm{CeO}_{2-\delta_{\mathrm{ox}}} + \mathrm{H_2/CO}, \tag{1.1}$$

where δ_{red} and δ_{ox} are the oxygen non-stoichiometry after reduction and oxidation, respectively and $\Delta\delta = \delta_{\mathrm{red}} - \delta_{\mathrm{ox}}$. This oxidation typically takes place at temperatures around 873–1373 K [8,16–18]. To regenerate the redox material's capacity to split water or carbon dioxide, it is reduced thermally using concentrated solar radiation. At temperatures in the order of 1773 K [8,19,20], oxygen is released from the redox material's lattice:

$$\frac{1}{\Delta\delta}\mathrm{CeO}_{2-\delta_{\mathrm{ox}}} \rightleftharpoons \frac{1}{\Delta\delta}\mathrm{CeO}_{2-\delta_{\mathrm{red}}} + \frac{1}{2}\mathrm{O_2}. \tag{1.2}$$

Major drawbacks of the process are caused by the high reduction temperature and the large temperature difference between the process steps: The high temperature results in large radiation losses and the heating of the redox material from the oxidation to the reduction temperature requires large amounts of high-temperature heat. The latter point is even emphasised since despite the high reduction temperature, relatively low reduction extents are achieved and thus large amounts of the redox material are needed. Operation under vacuum conditions [8,21], with a sweep gas [16,19,22–24], or more recently thermochemical pumping [25–28] and adsorption/desorption cycles [29–31] have been considered to decrease the oxygen partial pressure and thereby support the reduction [6,32]. Alternatively, a gaseous reductant can be introduced that reacts with the released oxygen creating a considerably lower partial pressure of oxygen than sweep gas and vacuum pumping [33]. Consequently, thermodynamically much higher reduction extents can be achieved even at reduced reduction temperatures [17,34]. Throughout the present work we will refer to the reduction using sweep gas, vacuum pumps or thermochemical pumps in combination to high temperatures as thermal reduction and to reduction with a gaseous reductant as thermochemical reduction. Alkanes like methane are suitable reductants. The reaction of the thermochemical reduction step with an alkane as a reductant is given by

$$\frac{1}{\Delta\delta}\mathrm{CeO}_{2-\delta_{\mathrm{ox}}} + \frac{1}{N}\mathrm{C}_N\mathrm{H}_{2N+2} \rightleftharpoons \frac{1}{\Delta\delta}\mathrm{CeO}_{2-\delta_{\mathrm{red}}} + \mathrm{CO} + \left(1+\frac{1}{N}\right)\mathrm{H_2}. \tag{1.3}$$

With methane as a reductant (N = 1), the net reaction of a two-step thermochemical redox cycle according to Reactions (1.1) and (1.3) is equal to steam methane reforming (SMR) in case of water splitting in the oxidation step or dry methane reforming (DMR) in case of carbon dioxide splitting. Therefore, this process is commonly referred to as redox reforming. Redox reforming of natural gas is frequently studied [17,35–41]. The disadvantage is that the use of natural gas introduces a fossil carbon source and the process is not carbon neutral – in contrast to a redox cycle with a purely thermal reduction step.

Solar production of H_2 and/or CO in a two-step redox cycle with a purely thermal reduction step was studied theoretically and experimentally [23,42–45]. The most mature reactor technology for this kind of process are discontinuous reactors with a directly irradiated monolithic redox structure. Marxer et al. [8] studied the performance of a 4 kW reactor at up to 1773 K. With their experimental setup they reached a solar-to-fuel efficiency of 5.25% for the conversion of CO_2 to CO. A major drawback of discontinuous reactors is that in each cycle, when heating the reactive material from the oxidation to the reduction temperature, other parts of the reactor such as the insulation are also heated to some extent, increasing the heat demand. Marxer et al. [8] found that 62.8% of the heat input into their system was required for this heating step. This reactor concept was later scaled up to 50 kW and the whole process from concentration of solar radiation *via* on-sun operation of the 50 kW redox reactor to production of a liquid fuel using a Fischer-Tropsch unit was demonstrated in field [2,46].

For the scale up of these batched receiver-reactors, the use of multiple reactors in staggered operational modes, so called reactor arrays, was investigated in recent years [47–49]. Arrays of discontinuous reactors allow a quasi-continuous production of syngas during sun hours, which is beneficial for the operation of downstream processes such as FT synthesis. Operational strategies for reactor arrays were investigated by Brendelberger et al. [47], based on the performance of a single reactor. Expected off-design conditions for a significant share of reactors within an array can reduce the efficiency to 57%–83% of the value for a single receiver reactor at the design point, depending on the selected strategy [47]. This value is referred to as array efficiency. Oberkirsch et al. [49] investigated receiver control strategies, using a neural network, which was trained with a reactor model by Grobbel et al. [48], resulting in array efficiencies of up to 79%.

Continuous reactor designs based on rotating elements, particles or other moving elements were suggested to overcome abovementioned disadvantages of discontinuous reactors. Many of these concepts also include a solid-solid heat exchanger reducing the sensible heat demand [21,50–56]. However, no such heat exchanger design was yet experimentally proven to reliably and reproducibly reach high heat recovery rates at the relevant temperature levels. In addition, undesired oxygen crossover within a solid-solid heat exchanger might occur, decreasing the efficiency of the solar redox cycle [57].

Process simulations of redox reforming with iron-oxide based redox materials were performed by Sheu et al. [35,36], who investigated hybrid solar-fossil processes for power generation. In such processes, solar redox DMR or SMR is used to convert natural gas and CO_2 or H_2O to syngas which has a higher heating value than the natural gas, thereby adding a solar share of energy to the fuel, which is then converted to power in a gas-fired power plant. He et al. [37] studied solar redox SMR for the coproduction of H_2 and liquid fuels *via* Fischer Tropsch synthesis. They also used an iron-oxide based redox material for experiments and process simulations and suggest the combustion of gaseous FT products supplemented with methane as an option to ensure continuous operation in absence of sunlight. This is however not further discussed. Warren et al. [17] studied redox reforming using ceria as a redox material both theoretically and experimentally using an indirectly irradiated reactor. Another experimental study of methane reforming was performed by Welte et al. [38], who reduced ceria with methane in a 2 kW_{th} reactor. Herein co-current and counter-current flow of ceria and methane through an Al_2O_3 tube were performed. The reaction of ceria and product gas, was found to be the main drawback of a counter-current arrangement. Process simulations performed by Holzemer-Zerhusen et al. [39] compare the performance of iron oxide and ceria-based redox reforming. Results show that solar redox reforming can be performed efficiently with temperature gaps between reduction and oxidation that are significantly lower than in solar-thermal water or CO_2-splitting cycles. Ceria showed much better selectivity towards syngas than iron oxide. The study also showed that solar redox reforming of natural gas is not necessarily more efficient than solar reforming over a conventional catalyst.

Another challenge is the formation of by-products during the conversion of the solar syngas to the final product. In fuel production *via* a Fischer-Tropsch process for example, the overall product consists not only of hydrocarbons of the desired chain length range. Instead, also a significant amount of short-chain gaseous hydrocarbons and waxes are produced. The waxes contain paraffinic hydrocarbons with very long chain lengths that are solid at standard conditions. They can be further processed using catalytic cracking or hydrocracking, which can yield high quality fuels through isomerization [58–60]. The gaseous

by-products on the other hand can often not be used on site. Therefore, the stream of gaseous hydrocarbons should ideally be recycled in order to generate new syngas for the fuel synthesis process to avoid flaring these gases and increasing the carbon efficiency. Falter et al. [61] suggested to treat gaseous short-chained by-products of the Fischer-Tropsch process with a steam reformer, reconverting it to syngas, which can be looped back into the Fischer-Tropsch reactor. Fan et al. [62] describe the use of a redox material to treat C_1–C_4 FT by-products in a Coal-to-Liquids process. Here a redox material, such as iron oxide is reduced, while the hydrocarbons are converted to CO_2 and steam. The CO_2 is not utilized and has to be sequestered or would otherwise be emitted into the environment. The steam could be used for power generation in a steam turbine [63]. Re-oxidation of the redox material with steam generates H_2 which is fed to the FT synthesis [62,63]. Adelung et al. [64] investigated a reverse-water gas shift (RWGS) reactor for syngas generation followed by FT synthesis and suggested to burn the gaseous FT products to provide heat for the RWGS reaction. An oxyfuel burner is used for the combustion of gaseous FT products. Generated CO_2 is fed back to the RWGS reactor after a monoethanolamine absorption. This concept results in a carbon efficiency of 88%.

In the present work, we suggest a different approach, which combines the advantages of a renewable redox cycle and redox reforming, while reusing FT by-products in the redox cycle. As depicted in Fig. 1, the by-products are fed to the reduction step of the redox cycles. Here they act as reductant for a share of the redox material, which allows higher degrees of reduction, lower reduction temperatures and higher operation pressures. The by-products can be partially oxidized and thereby directly converted to syngas (CO and H_2) or they are fully oxidized to CO_2 and H_2O, which can be fed to the oxidation step, where they are converted to syngas. Using the by-products as a reductant, they are not only recycled and later on converted to the desired product, but also the energy demand of the reduction step, which causes a large portion of the process' overall energy demand, can be decreased considerably. The main steps of the suggested approach and their respective function are summarised in Table 1.

In the framework of the present study we focus on a ceria-based redox cycle, coupled to a Fischer-Tropsch process, in which the gaseous short-chained by-products methane, ethane, propane and butane are utilized as reductants. The process is however generally not limited to this setup and can also be used with other synthesis processes, which convert syngas and produce undesired by-products, which are suitable candidates for the reduction of a redox material. The study aims to evaluate the potential of the concept, assessing the reduction effectiveness, energy savings and product composition of the modified reduction step, for a simplified process design.

Table 1
Main process steps of the suggested novel approach and their respective function.

Process step	Function
Oxidation	Oxidation of redox material with H_2O and CO_2, forming H_2 and CO (Reaction (1.1)).
Fuel synthesis	Fuel synthesis step, e.g. Fischer-Tropsch-process, forming hydrocarbons from H_2 and CO. Short-chained volatile hydrocarbons are produced as an unwanted by-product.
Hydrocarbon recycling	Volatile hydrocarbons are used as a reductant in the reduction of the redox material. Utilization of these hydrocarbons aims to significantly increase the carbon efficiency. Increased carbon efficiency can lead to a downscaled redox cycle (at same fuel production rate), which is expected to result in improved energy efficiency.
Reduction	Reduction is split into a thermal reduction and a thermochemical reduction.
Thermal reduction	Separates O_2 from the redox material at a high temperature (Reaction (1.2)). Is needed if not all the redox material is reduced thermochemically.
Thermochemical reduction	Separates O_2 from the redox material with the help of a reductant (Reaction (1.3)). Aims to reduce energy demand of reduction, due to beneficial operation conditions such as reduced temperature, increased oxygen non-stoichiometry or increased pressure.

2. Methodology

In the present study, we investigate the potential of the proposed thermochemical reduction on the basis of a continuously operated process. Herein ceria is used as a redox material and is cycled between reduction and oxidation reactors, for example in the form of particles or mobile monolithic structures. For the reduction, a reactor array is assumed to be available such that the available amount of short-chained alkanes can be freely distributed between the reactors. The short-chained alkanes are a by-product of a Fischer-Tropsch synthesis which is considered as a coupled fuel-synthesis process. Note that the generic model for the thermochemical reduction and the results described in this work are typically also applicable for other continuous reactor designs that allow co-feeding of the solid and gaseous reactants and the free adjustment of the ratio of reductant to redox material. For the sake of

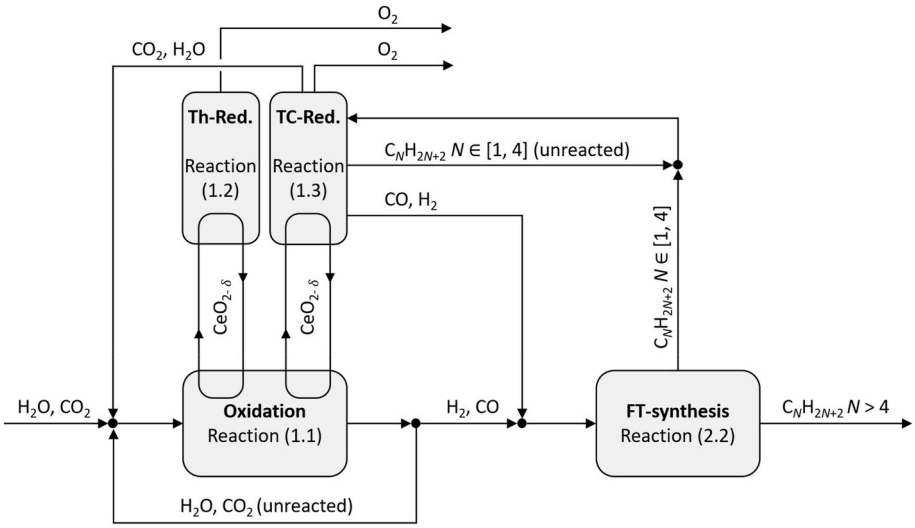

Fig. 1. Schematic of the suggested novel approach. Th-Red.: thermal reduction, TC-Red.: thermochemical reduction.

readability, our explanations will however be exemplified with only one implementation, namely the reactor array mentioned above.

2.1. Material balances

A common approach to describe the product spectrum of Fischer-Tropsch synthesis is the Anderson–Schulz–Flory (ASF) distribution. The molar fraction x_N of a component with a specific carbon number N is related to the probability of chain growth α [58]:

$$x_N = (1-\alpha)\,\alpha^{N-1}. \tag{2.1}$$

The probability of chain growth α and thereby the obtained product spectrum is defined by the process conditions. Higher process temperatures lead to a lower chain growth probability due to the increased Brownian motion. Therefore, a higher process temperature shifts the product spectrum to shorter carbon chains and increases the amount of gaseous hydrocarbons in the product. Two general operational modes of Fischer-Tropsch synthesis exist: high and low temperature Fischer-Tropsch synthesis (HTFT and LTFT). Industrial HTFT is operated at 573–623 K and LTFT at 473–523 K [59]. The α-value for HTFT is in the range of 0.65–0.70 and for LTFT in the range of 0.84–0.92 [58].

The product spectrum of the FT synthesis comprises a wide range of hydrocarbons and oxygenates of different chain sizes. To reduce the complexity, in this analysis the FT product is regarded as a mixture of alkanes. Equation (2.2) shows the overall Fischer-Tropsch product formation reaction for alkanes from hydrogen and carbon monoxide with a stochiometric H_2:CO ratio of approximately 2:1 [58,59]:

$$(2N+1)\,H_2 + N\,CO \rightarrow C_NH_{2N+2} + N\,H_2O. \tag{2.2}$$

Since the total number of carbon atoms is a constant throughout the process, it is helpful to introduce a carbon atom-based molar flow rate $\dot{n}_{c,N}$ for balance equations, where e.g. 1 mol/s of $C_{10}H_{12}$ equals 10 mol_c/s. The fraction of a species with N carbon atoms with respect to the overall number of carbon atoms is denoted as $f_{c,N} = \dot{n}_{c,N}/\dot{n}_c$. Similar to x_N, $f_{c,N}$ can be determined by the ASF distribution according to [58]

$$f_{c,N} = N\,(1-\alpha)^2\,\alpha^{N-1}. \tag{2.3}$$

To understand how much reductant is available in the process, we balance the amount of carbon. Here, the FT product distribution is important and we summarize the fractions of short-chained alkanes that can be used as reductant, namely C_1–C_4 alkanes, into the quantity φ, with

$$\varphi = f_{c,1} + f_{c,2} + f_{c,3} + f_{c,4} \tag{2.4}$$

being the portion of the FT product that is recycled within the process. For simplicity of the reactor models, the material flow of reductant is modelled as an equivalent methane flow, as is explained in more detail in Section 2.2.

According to Fig. 2 (a), the following balance equations can be derived:

$$\dot{n}_{c,F} = \dot{n}_{c,P}, \tag{2.5}$$

$$\dot{n}_{c,red} = \dot{n}^{TC}_{CH_4} + \left(\dot{n}_{c,F} + \dot{n}^{TC}_{CO_2} + \dot{n}^{TC}_{CO}\right)\varphi. \tag{2.6}$$

Using the methane conversion in the thermochemical reduction X_{CH_4} with

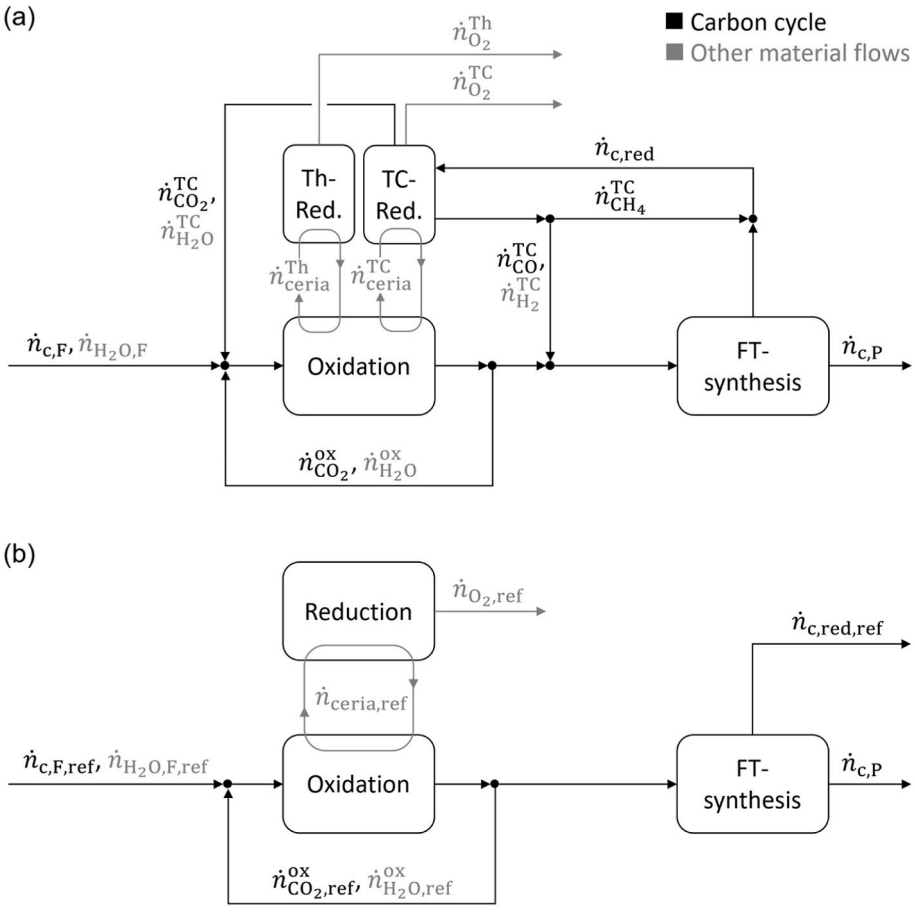

Fig. 2. Schematic of the carbon cycle and other material flows within the process for (a) the suggested novel approach and (b) the reference case. Th-Red.: thermal reduction, TC-Red.: thermochemical reduction.

$$\dot{n}^{\mathrm{TC}}_{\mathrm{CH_4}} = \left(1 - X_{\mathrm{CH_4}}\right) \dot{n}_{\mathrm{c,red}} \tag{2.7}$$

and

$$\dot{n}^{\mathrm{TC}}_{\mathrm{CO_2}} + \dot{n}^{\mathrm{TC}}_{\mathrm{CO}} = X_{\mathrm{CH_4}}\, \dot{n}_{\mathrm{c,red}} \tag{2.8}$$

the amount of recycled reductant can be calculated as

$$\dot{n}_{\mathrm{c,red}} = \frac{\varphi}{X_{\mathrm{CH_4}}\,(1-\varphi)}\, \dot{n}_{\mathrm{c,F}}. \tag{2.9}$$

Fig. 2 (b) shows a reference case without recycling of short-chained hydrocarbons. According to Fig. 2 (b) and Equation (2.5), the carbon-based feed $\dot{n}_{\mathrm{c,F,ref}}$ that would be needed to produce the same amount of product $\dot{n}_{\mathrm{c,P}}$ is given by

$$\dot{n}_{\mathrm{c,F,ref}} = \frac{\dot{n}_{\mathrm{c,F}}}{1-\varphi}. \tag{2.10}$$

The purpose of the reduction step is to create oxygen vacancies in the redox material, which enable the material to split water and CO_2 in the oxidation step. In our novel approach, part of these vacancies is created in a thermochemical (TC) reduction step. However, a portion of the redox material still has to be reduced thermally (Th) as in the reference case. To quantify the amount of vacancies that have to be created thermochemically and thermally, we introduce the vacancy ratio Φ:

$$\Phi^{\mathrm{TC}} = \frac{\Delta\delta^{\mathrm{TC}}\, \dot{n}^{\mathrm{TC}}_{\mathrm{ceria}}}{\Delta\delta_{\mathrm{ref}}\, \dot{n}_{\mathrm{ceria,ref}}}, \tag{2.11}$$

$$\Phi^{\mathrm{Th}} = \frac{\Delta\delta^{\mathrm{Th}}\, \dot{n}^{\mathrm{Th}}_{\mathrm{ceria}}}{\Delta\delta_{\mathrm{ref}}\, \dot{n}_{\mathrm{ceria,ref}}}, \tag{2.12}$$

where the expression in the denominator refers to the reference case without recycling in Fig. 2 (b). Hence, the vacancy ratio describes the number of vacancies that has to be created in the thermal and thermochemical reduction, respectively, compared to the vacancies created thermally in the reference case. The number of vacancies created in the reference case follows directly from the feed stream. $\Delta\delta^{\mathrm{TC}}$ is calculated in equilibrium calculations which are described below. $\dot{n}^{\mathrm{TC}}_{\mathrm{ceria}}$ can be expressed using the ratio of ceria to reductant, which is an input parameter in the equilibrium calculations. This yields

$$\Phi^{\mathrm{TC}} = \frac{\Delta\delta^{\mathrm{TC}} \left(\frac{\dot{n}^{\mathrm{TC}}_{\mathrm{ceria}}}{\dot{n}_{\mathrm{c,red}}}\right)_{\mathrm{EQ}} \dot{n}_{\mathrm{c,red}}}{3\, \dot{n}_{\mathrm{c,F,ref}}}, \tag{2.13}$$

where the index EQ refers to a molar ratio, calculated or used as an input parameter in the equilibrium model, described in Section 2.3. The factor 3 accounts for the fact that with each carbon atom, which is converted in the oxidation step, also two water molecules are converted to hydrogen to maintain the desired H_2:CO ratio of 2:1. Hence, 3 oxygen atoms are taken up by ceria per converted carbon atom. The H_2:CO ratio is achieved by splitting both H_2O and CO_2 in the oxidation. Using Equation (2.9), (2.10) and (2.13) results in

$$\Phi^{\mathrm{TC}} = \frac{\varphi}{3\, X_{\mathrm{CH_4}}}\, \Delta\delta^{\mathrm{TC}} \left(\frac{\dot{n}^{\mathrm{TC}}_{\mathrm{ceria}}}{\dot{n}_{\mathrm{c,red}}}\right)_{\mathrm{EQ}}. \tag{2.14}$$

During the thermochemical reduction, methane can be oxidized partially to syngas (SG), containing CO and H_2, or fully to its combustion products (CP) CO_2 and H_2. The number of oxygen vacancies is linked to the amount of CO, CO_2, H_2O and O_2 produced in the thermochemical reduction:

$$\Delta\delta^{\mathrm{TC}}\, \dot{n}^{\mathrm{TC}}_{\mathrm{ceria}} = \dot{n}^{\mathrm{TC}}_{\mathrm{CO}} + 2\, \dot{n}^{\mathrm{TC}}_{\mathrm{CO_2}} + \dot{n}^{\mathrm{TC}}_{\mathrm{H_2O}} + 2\, \dot{n}^{\mathrm{TC}}_{\mathrm{O_2}}. \tag{2.15}$$

To distinguish between oxygen vacancies that are associated with conversion of methane to syngas and such that result from conversion of methane to its combustion products we introduce

$$\Phi^{\mathrm{TC}}_{\mathrm{SG}} = \frac{\varphi}{3\, X_{\mathrm{CH_4}}} \left(\frac{\dot{n}^{\mathrm{TC}}_{\mathrm{CO}}}{\dot{n}_{\mathrm{c,red}}}\right)_{\mathrm{EQ}} \tag{2.16}$$

and

$$\Phi^{\mathrm{TC}}_{\mathrm{CP}} = \frac{\varphi}{3\, X_{\mathrm{CH_4}}} \left(2 \left(\frac{\dot{n}^{\mathrm{TC}}_{\mathrm{CO_2}}}{\dot{n}_{\mathrm{c,red}}}\right)_{\mathrm{EQ}} + \left(\frac{\dot{n}^{\mathrm{TC}}_{\mathrm{H_2O}}}{\dot{n}_{\mathrm{c,red}}}\right)_{\mathrm{EQ}}\right). \tag{2.17}$$

According to Equation (2.15), the total thermochemical vacancy ratio Φ^{TC} also contains an expression for O_2, which is neither included in $\Phi^{\mathrm{TC}}_{\mathrm{SG}}$ nor in $\Phi^{\mathrm{TC}}_{\mathrm{CP}}$. For many points of operation, the oxygen concentration in the product stream of the thermochemical reduction is however very low. Therefore,

$$\Phi^{\mathrm{TC}} \approx \Phi^{\mathrm{TC}}_{\mathrm{SG}} + \Phi^{\mathrm{TC}}_{\mathrm{CP}} \tag{2.18}$$

holds for most points of operation.

Vacancies created by thermal reduction, are the total of all vacancies needed to convert 3 $\dot{n}_{\mathrm{c,F}}$, $\dot{n}^{\mathrm{TC}}_{\mathrm{CO_2}}$ and $\dot{n}^{\mathrm{TC}}_{\mathrm{H_2O}}$ according to Fig. 2 (a) minus the vacancies that were already create thermochemically. The latter are given in Equation (2.15). Using the conversion of reducing agent, the vacancy ratio for the thermal reduction Φ^{Th} reads

$$\Phi^{\mathrm{Th}} = \frac{3\, \dot{n}_{\mathrm{c,F}} - X_{\mathrm{CH_4}}\, \dot{n}_{\mathrm{c,red}} - 2\, \dot{n}^{\mathrm{TC}}_{\mathrm{O_2}}}{3\, \dot{n}_{\mathrm{c,F,ref}}}. \tag{2.19}$$

For Φ^{Th} it is not relevant, whether the reducing agent is converted to a syngas (CO + H_2) or the combustion products (CO_2 + H_2O) in the thermochemical reduction. The reason for this is that conversion to the combustion products does increase the number of vacancies created thermochemically, but at the same time these additional vacancies are needed to convert CO_2 and H_2O to CO and H_2 in the oxidation step as depicted in Fig. 2 (a). Therefore, the same amount of thermally create vacancies is necessary to convert the feed stream $\dot{n}_{\mathrm{c,F}}$. Using Equations (2.9) and (2.10), Equation (2.19) can be rearranged to

$$\Phi^{\mathrm{Th}} = (1-\varphi) \left(1 - \frac{\varphi}{3\,(1-\varphi)} - \frac{2\, \dot{n}^{\mathrm{TC}}_{\mathrm{O_2}}}{3\, \dot{n}_{\mathrm{c,F}}}\right). \tag{2.20}$$

Similarly to the amount of CO, CO_2 and H_2O in Equations (2.16) and (2.17), the amount of O_2 can be expressed *via* the ratio of O_2 to reductant in the equilibrium calculations, i.e.

$$\frac{\dot{n}^{\mathrm{TC}}_{\mathrm{O_2}}}{\dot{n}_{\mathrm{c,F}}} = \left(\frac{\dot{n}^{\mathrm{TC}}_{\mathrm{O_2}}}{\dot{n}_{\mathrm{c,red}}}\right)_{\mathrm{EQ}} \frac{\dot{n}_{\mathrm{c,red}}}{\dot{n}_{\mathrm{c,F}}}. \tag{2.21}$$

Equation (2.20) can then be rewritten using Equation (2.21) and again Equation (2.9) to

$$\Phi^{\mathrm{Th}} = 1 - \frac{4\,\varphi}{3} - \frac{2\,\varphi}{3\, X_{\mathrm{CH_4}}} \left(\frac{\dot{n}^{\mathrm{TC}}_{\mathrm{O_2}}}{\dot{n}_{\mathrm{c,red}}}\right)_{\mathrm{EQ}}. \tag{2.22}$$

2.2. Reducing agent

Methane is used as a representative of short chained hydrocarbons that can be used as a reductant. The available molar amount of methane is approximated to be that of carbon atoms in all C_1–C_4 alkanes combined. This assumption is in line with an oxygen balance for Reaction (1.3). Since in this reaction, the number of oxygen atoms removed from the redox material only depends on the number of carbon atoms, a mixture of for example 1 mol C_1H_4 and 1 mol C_2H_6 can reduce ceria to the same extent as 3 mol of C_1H_4. However, the chemical potentials of the different hydrocarbons, result in different reaction equilibria. Fig. 3 shows $\Delta_R G^\circ$ of the oxidation of the relevant alkanes. For reference, the expression $-R\,T\ln(K)$ for equal conversion of oxygen in all four reactions is included. Herein K is the equilibrium constant of reactions R1 – R4, given in the figure. Due to the different stoichiometric factors, this

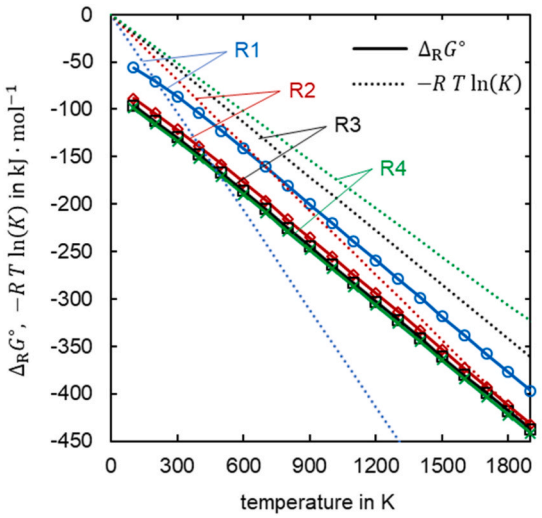

R1 $CH_4 + \frac{1}{2}O_2 \rightarrow CO + 2H_2$

R2 $\frac{1}{2}C_2H_6 + \frac{1}{2}O_2 \rightarrow CO + \frac{3}{2}H_2$

R3 $\frac{1}{3}C_3H_8 + \frac{1}{2}O_2 \rightarrow CO + \frac{4}{3}H_2$

R4 $\frac{1}{4}C_4H_{10} + \frac{1}{2}O_2 \rightarrow CO + \frac{5}{4}H_2$

Fig. 3. Illustration of the chemical equilibrium of the partial oxidation of different hydrocarbons derived from the concept of an Ellingham diagram. The intercept of $\Delta_R G^\circ$ and $-R\,T\,\ln(K)$ specifies the equilibrium of a reaction for that value of K. Data from *FactSage* 7 with database *FactPS*.

value is different for each reaction, resulting in different slopes for $-R\,T\,\ln(K)$. The intercept of $\Delta_R G^\circ$ and $-R\,T\,\ln(K)$ denotes the equilibrium of a reaction.

The graph shows that the same conversion of oxygen is achieved with ethane at a higher temperature compared to methane and at an even higher temperature for propane and butane. Given that the reactions are exothermal, this means that at the same temperature, the longer chained alkanes (C_2–C_4) can achieve a higher conversion suggesting they are better reductants than methane and our approach to model the reductant as pure methane stream is a conservative estimate. The desired product of the thermochemical reduction is syngas. As a side reaction however, full oxidation of the reductant to its combustion products CO_2 and H_2O is possible. In this case, the reduction extent depends not only on the number of carbon atoms, but also on the number of hydrogen atoms according to

$$\frac{3+\frac{1}{N}}{\Delta\delta}CeO_{2-\delta_{ox}} + \frac{1}{N}C_NH_{2N+2} \rightleftharpoons \frac{3+\frac{1}{N}}{\Delta\delta}CeO_{2-\delta_{red}} + CO_2 + \left(1+\frac{1}{N}\right)H_2O. \tag{2.23}$$

Hence, methane might be a somewhat better reductant due to the higher hydrogen to carbon ratio, when conversion to combustion product takes place.

2.3. Reactor modelling

We use zero-dimensional reactor models in which chemical equilibria are assumed to be established. The thermochemical reduction is modelled in *Aspen Customer Modeler* V10 [39]. For energetic calculations a *Python* model [57] is used, in which the equilibrium of the oxidation reaction is calculated with thermodynamic data from *FactSage* 7 with the database *FactPS*. The equilibrium composition can be calculated with the Gibbs free energy according to

$$\Delta_R G^\circ = -RT\ln\left(\prod_i \frac{\phi_i\, p_i}{p^\circ}^{\nu_i}\right), \tag{2.24}$$

where ϕ_i is the fugacity coefficient of component i. In reactions that involve the redox material, due to the non-stoichiometric behaviour of ceria, $\Delta_R G^\circ$ is a function of δ, which changes over the course of the reaction. Hence, Equation (2.24) cannot be applied to such reactions directly. Instead, Reaction (1.3) can be interpreted as the sum of Reaction (1.2) and the gas-phase reaction

$$CH_4 + \frac{1}{2}O_2 \rightleftharpoons CO + 2\,H_2. \tag{2.25}$$

Similarly, Reaction (1.1) is the sum of

$$H_2O \,/\, CO_2 \rightleftharpoons H_2 \,/\, CO + \frac{1}{2}O_2 \tag{2.26}$$

and the reverse of Reaction (1.2). Equation (2.24) can then be used for the two gas-phase reactions (2.25) and (2.26), while Reaction (1.2) and its reverse reaction are described with a correlation by Bulfin et al. [9]. For the thermochemical reduction, Reaction (2.26) and the water-gas shift reaction

$$CO + H_2O \rightleftharpoons CO_2 + H_2 \tag{2.27}$$

are considered as side reactions.

The necessary amount of ceria is directly linked to the amount of oxidation product $\dot{n}_{prod,ox}$, i.e. H_2 and CO and scales with the difference in δ-values in reduction and oxidation $\Delta\delta$, according to

$$\dot{n}_{ceria} = \frac{\left(\dot{n}_{prod,ox} - 2\,\dot{n}_{O_2,ox}\right)}{\Delta\delta}, \tag{2.28}$$

where $\dot{n}_{O2,ox}$ denotes the amount of oxygen left in the product stream, which is however virtually zero as almost all oxygen is removed from the gas phase by ceria. Heating ceria from the oxidation to the reduction temperature results in an energy demand $\dot{Q}_{ceria}$, defined by

$$\dot{Q}_{ceria} = \dot{n}_{ceria}\int_{T_{ox}}^{T_{red}} c_{p,ceria}\,\mathrm{d}T. \tag{2.29}$$

The reaction enthalpy of the thermal reduction according to Reaction (1.2) depends on δ and can be obtained by

$$\Delta_R\dot{H}^{Th}_{red} = \dot{n}_{ceria}\int_{\delta_{ox}}^{\delta_{red}} \Delta_\delta h(\delta)\,\mathrm{d}\delta, \tag{2.30}$$

where $\Delta_\delta h(\delta)$ is the incremental change of the reaction enthalpy with respect to δ, calculated with a polynomial by Bulfin et al. [65] fit to data by Panlener et al. [6]. In case of the thermochemical reduction, the reaction enthalpy can be written as the sum of the reaction enthalpies of the thermal reduction step and the exothermal gas phase reaction (2.25):

$$\Delta_R\dot{H}^{TC}_{red} = \Delta_R\dot{H}^{Th}_{red} + \dot{n}_{prod,ox}\,\Delta_R h_{gas}, \tag{2.31}$$

with $\Delta_R h_{gas} < 0$, calculated in *FactSage* 7. The reaction enthalpy for the conversion of CH_4 to CO_2 and H_2O is neglected, because in the energy assessment in Chapter 3.5, only points of operation are investigated in which CH_4 is almost fully converted to CO and H_2.

Heat losses of the reactors are assumed to be limited to radiative heat losses and are considered by means of the ideal efficiency for a black-body receiver

$$\eta_{rec} = 1 - \frac{\sigma \left(T_{red}^4 - T_{amb}^4\right)}{I_{sol}\, C}, \tag{2.32}$$

where σ is the Stefan-Boltzmann constant, I_{sol} is the insolation and C is the concentration factor. From that, heat losses can be calculated as

$$\dot{Q}_{loss} = \left(\frac{1}{\eta_{rec}} - 1\right)\left(\dot{Q}_{ceria} + \Delta_R \dot{H}_{red}\right). \tag{2.33}$$

More details on the described models can be found in Refs. [39,57].

3. Simulation results and discussion

In the following, we investigate the effect of adding a reductant on the performance of the reduction step. For comparison, a reference case with a purely thermal reduction step is defined. The impact of our novel approach on reduction extent δ_{red} and reduction temperature T_{red}, the number of thermochemically and thermally created oxygen vacancies, represented by Φ^{TC} and Φ^{Th}, the energy savings for the reduction step and the product composition of the thermochemical reduction are discussed. Parameters for the reference case are listed in Table 2. Since the new concept only affects the reduction, parameters of the oxidation reactors are the same for reference case and novel approach.

3.1. Reduction performance

As shown in Fig. 4 (a), the reduction extent can be increased drastically if enough reductant is used in the reduction step. Hence, the same amount of syngas can be produced with less ceria, which reduces the sensible heat needed to heat ceria from the oxidation to the reduction temperature, which amounts to 66% of the overall heat demand of the reduction step in the reference process. Fig. 4 (a) also reveals that for a large range of the reductant amount, the total pressure in the reduction reactor has virtually no effect on δ_{red}. At a reductant amount close to zero however, the vacuum case performs better than the high-pressure cases. In this region, δ_{red} approaches the value of a purely thermal reduction step, in which δ_{red} is considerably higher if a low total pressure is set, which in this case equals the oxygen partial pressure. Therefore, a certain amount of reductant is needed for the higher pressures to reach a higher δ_{red} than the reference case without reductant, represented by a dotted black line in the illustration. The difference between operation at atmospheric pressure and at 20 bar is negligible.

The expression of δ as a function of temperature and pressure by Bulfin et al. [9] that was used in the present study is a semi empirical approach, which was fit to data by Panlener et al. [6] and Zinkevich et al. [66] in the p_{O_2}-range of 10^{-2} to 10^{-9} bar. However, the physical basis of the equation allows extrapolation over the range of these p_{O_2}-values to a certain degree, as long as δ is not too high. In fact, for calculations with $\delta_{red} = 0.025$, such as in Fig. 4 (b), we find the results to be in good agreement with data presented in Ref. [66], even for a p_{O_2} as low as 10^{-29} bar. Also, for the calculations with variable δ_{red} at $T_{red} = 1791$ K, for example in Fig. 4 (a), the results are in good agreement with abovementioned data for values of δ_{red} up to approximately 0.32 which correlates to approximately $p_{O_2} = 10^{-13}$ bar. Even higher values of δ_{red} are however not possible, even though they might be predicted by the model, as such a strong reduction would cause an undesirable phase change of the cerium oxide [66], which is not investigated in the present study.

Table 2
Parameters of the reference case. $T_{red,ref}$ and X_{ox} are chosen such that they match $\delta_{red,ref}$ and δ_{ox}.

Parameter	Meaning	Value
$\delta_{red,ref}$	Oxygen non-stoichiometry after reduction	0.025
δ_{ox}	Oxygen non-stoichiometry after oxidation	0.005
$p_{O_2,red,ref}$	Oxygen partial pressure in reduction reactors	10^{-3} bar
p_{ox}	Total pressure in oxidation reactors	1.01325 bar
T_{ox}	Temperature in oxidation reactors	1073 K
$T_{red,ref}$	Temperature in reduction reactors	1791 K
X_{ox}	Conversion of H_2O or CO_2 in oxidation reactors	0.21
$I_{sol}\, C$	Concentrated solar flux entering receiver reactors	2.5 MW m^{-2}

Utilizing a reductant, it is possible to increase the reduction extent and/or decrease the reduction temperature. In the following, we discuss an operation of the reactors with reductant at lower temperatures and the same degree of reduction δ_{red} as in the purely thermal reduction. The results are given in Fig. 4 (b). Lower reduction temperatures significantly reduce reradiation losses of the receiver, which are proportional to T_{red}^4. Also, at lower reduction temperatures, the gap between oxidation and reduction temperature decreases and hence less sensible heat is needed to heat up ceria after the oxidation.

Fig. 4 (b) shows the reduction temperature T_{red} as a function of the amount of reductant per mol of ceria, which is fed into the reactors. Herein our standard reference case from Table 2 is compared to operation with reductant. In all cases, $\delta_{red} = 0.025$. At low amounts of reductant, the necessary temperature decreases moderately before at around 0.005 mol CH_4 per mol ceria, a drastic temperature change is observed, whereas at higher reductant-amounts the temperature curve flattens again. This effect is caused by the strongly non-linear correlation between δ_{red}, T_{red} and $p_{O_2,red}$, the latter being a result of the amount of reductant and the respective chemical equilibrium. The impact of the total pressure in the reduction chamber in Fig. 4 (b) is most apparent for low reductant-amounts and negligible for a large portion of relevant points of operation. This again shows that high pressure operation of the thermochemical reduction might be a feasible option.

In summary, we find that a thermochemical reduction step can significantly increase δ_{red} or reduce T_{red}. Given these results, combination of increased δ_{red} and reduced T_{red} also seems to be a viable option. Finding the most suitable point of operation is an optimization problem the solution to which is beyond the scope of this study.

The vacancy ratios Φ^{TC} and Φ^{Th} represent the number of vacancies created in the thermochemical and thermal reduction step in the novel process, relative to the reference process. Therefore, Φ^{TC} and Φ^{Th} allow to quantify the potential energy benefits of the novel approach. Using Φ_{SG}^{TC} and Φ_{CP}^{TC} additionally reveals whether the reductant is converted to a syngas (H_2 + CO) or rather combustion products (H_2O + CO_2). Fig. 5 depicts the different vacancy ratios and the reductant conversion for the reduction at atmospheric pressure. Values for $p_{red} = 10^{-3}$bar and $p_{red} = 20$ bar are similar and point to the same general trends. As mentioned above, a reactor array allows to divide the reducing agent freely between the reactors, so that either a small amount of ceria can be reduced using large amounts of reducing agent or a larger amount of ceria can be reduced with smaller amounts of the reducing agent. The curves shown in Fig. 5 help to understand the process' behaviour at different ratios of reducing agent to ceria. This behaviour is explained in the following, starting at high ratios of methane to ceria moving to lower ratios, i.e. going from right to left in Fig. 5: At high methane-to-ceria ratios, the methane conversion is typically significantly below 1 and with respect to the vacancy ratios, $\Phi^{TC} \approx \Phi_{SG}^{TC}$ and $\Phi_{CP}^{TC} \approx 0$ is found. The latter means that virtually all of the reductant that is converted, is converted to H_2 and CO, while no H_2O and CO_2 are produced. This product composition can be explained with a shortage of oxygen, which results from the low quantities of ceria compared to the reducing agent.

Moving towards smaller ratios of methane to ceria, the conversion X_{CH_4} increases, while Φ^{Th} stays constant and in a certain range also Φ^{TC}

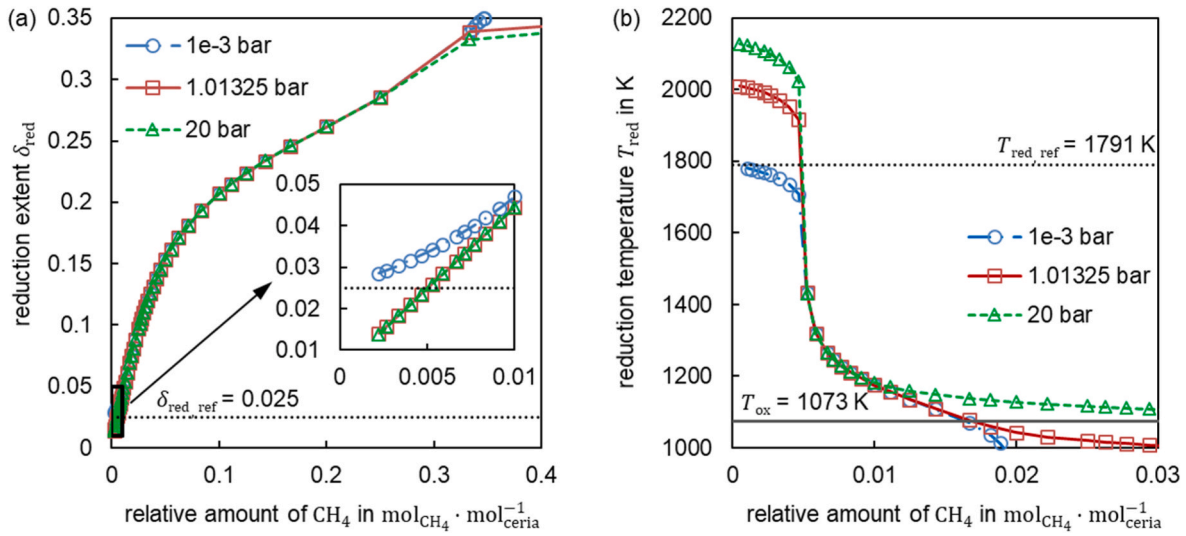

Fig. 4. Effect of adding reducing agent to the reduction reaction for different p_{red}. (a): reduction extent as a function of the amount of reducing agent at a constant reduction temperature of 1791 K, i.e. identical to the reference case. The dotted horizontal line shows the reduction extent of the refence process. (b): reduction temperature as a function of the amount of reducing agent at a constant reduction extent of 0.025, i.e. identical to the reference case. The horizontal lines show the reduction temperature of the refence process and the oxidation temperature, respectively.

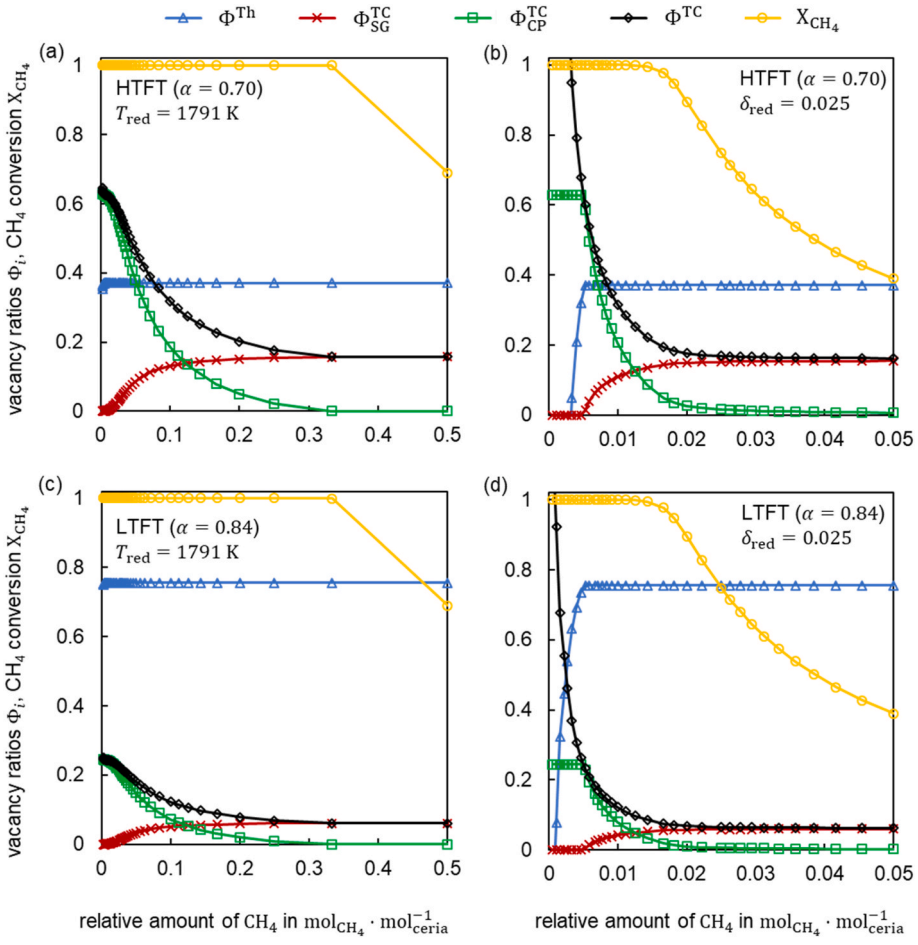

Fig. 5. Vacancy ratio and reductant conversion as a function of the relative amount of reductant, for both HTFT and LTFT at p_{red} = 1.01325 bar. Subfigures (a) and (c) show a case with variable δ_{red} and T_{red} = 1791 K as in Fig. 4 (a), whereas subfigures (b) and (d) show a case with variable T_{red} and δ_{red} = 0.025 as in Fig. 4 (b).

is almost constant. Constant Φ^{Th} and Φ^{TC} mean that the number of vacancies created thermally and thermochemically does not change with increasing X_{CH_4}. Reason for that is that unreacted CH_4 is cycled back into the thermochemical reduction reactors as indicated in Fig. 2 (a). Consequently, the total amount of converted CH_4 and therefore the amount of thermochemically created vacancies is independent of X_{CH_4},

which also follows from Equations (2.9) and (2.19).

At even lower methane-to-ceria ratios, Φ^{TC} and Φ^{TC}_{CP} increase, while Φ^{TC}_{SG} decreases, especially where $X_{CH_4} \approx 1$ is reached. Lower methane-to-ceria ratios imply larger quantities of ceria per mol of CH_4 and with that more oxygen is available to react with CH_4, which is why the conversion is high at low ratios of methane to ceria. Obviously, it is not possible to achieve more than full conversion and consequently, if even more oxygen is available than needed to reach almost full conversion of methane, this oxygen surplus results in a shift to reaction products that have a higher oxygen content, namely CO_2 and H_2O. The additional uptake of oxygen from the redox material increases Φ^{TC}, i.e. the number of vacancies created thermochemically. Interestingly, Φ^{Th} does not change and is still constant, meaning that the same number of thermally created vacancies is needed even though more vacancies are created by the thermochemical reduction. In other words, at these points of operation, the total number of necessary vacancies is higher. This effect is due to the fact that CO_2 and H_2O that are produced in the thermochemical reduction have to be converted to CO and H_2 in the oxidation step as depicted in Fig. 2 (a). For this, exactly the additionally created vacancies are needed. In fact, we find $1 - \varphi < \Phi^{TC} + \Phi^{Th} < 1$ to be fulfilled at all times. Since φ, as defined in Equation (2.4), is the fraction of short chained hydrocarbons in the FT product, it resembles the part that is cycled back in the novel approach as a reductant and is not used in the reference process. Hence, $\Phi^{TC} + \Phi^{Th} = 1 - \varphi$ means that the necessary number of vacancies in the novel process is reduced by the percentage of recycled FT product compared to the reference case. This reduction results from the fact that the short-chained hydrocarbons are not wasted and are instead converted to syngas and again fed to the FT synthesis. As a result, compared to the reference process, the feed stream $\dot{n}_{c,F}$ is reduced by the recycled reductant stream, or in relative measures by φ and with it the number of vacancies needed to convert the feed stream to syngas. This is however only the case, if the reductant is converted to a syngas consisting of only CO and H_2. If it is instead converted to the combustion products CO_2 and H_2O, additional vacancies are needed, as explained above, to react these combustion products to CO and H_2 in the oxidation step. For a case in which the reductant is fully converted to CO_2 and H_2O, $\dot{n}_{c,F}$ and the stream of CO_2 and H_2O that are both fed to the oxidation add up to the exact value of the feed stream of the reference process. Therefore, in such a case, the same number of vacancies would be needed in the novel approach and the reference process, i.e. $\Phi^{TC} + \Phi^{Th} = 1$. From this discussion we can conclude that there are no apparent benefits of a point of operation in which the reductant is converted to CO_2 and H_2O rather than CO and H_2. Conversion to the combustion products allows for more vacancies being created in the thermochemical reduction, but at the same time, these vacancies cannot be used to convert the feed stream to syngas and consequently the scale of energy intensive thermal reduction cannot be reduced. Additionally, the need to feed the combustion products to the oxidation step increases the dimensions of oxidation reactors and might require a more complex process design, including gas separation. An incomplete conversion in the thermochemical reduction step, i.e. $X_{CH_4} < 1$, also results in the need for gas separation and/or increased plant dimensions. Consequently, it appears to be the best option, to choose a ratio of reductant to ceria at which X_{CH_4} is close to 1 and Φ^{TC}_{CP} is close to 0.

At very low ratios of methane to ceria close to 0, Φ^{TC} rises to very high values, while Φ^{Th} drops drastically and can even fall below 0 as can be seen in Fig. 5 (b) and (d). In this region, large concentrations of O_2 can be found in the product of the thermochemical reduction. The low amount of reductant is not sufficient to reach a certain δ_{red}-value (in this case 0.025) and thus high temperatures are needed to release the oxygen from the solid as is depicted in Fig. 4 (b). At such high temperatures and low quantities of reducing agent, the thermochemical reduction has more the character of a thermal reduction in which oxygen is released as O_2. If very low ratios of methane to ceria are used, the available amount of reductant can be distributed over a large amount of ceria and thus more vacancies can be created in the thermochemical reduction than needed. Since Φ^{Th} is defined *via* the total number of vacancies needed in the process minus the vacancies already created thermochemically, such a point of operation results in $\Phi^{Th} < 0$. In this case the sum $\Phi^{TC} + \Phi^{Th}$ is more representative for the necessary number of vacancies than the individual terms Φ^{TC} and Φ^{Th} and $1 - \varphi < \Phi^{TC} + \Phi^{Th} < 1$ still holds. In fact, the sum of the two vacancy ratios is close to 1 in this region. Since the thermochemical reduction would in this case rather act like a thermal reduction, these very low ratios of methane to ceria do not resemble a reasonable point of operation as the novel process is rather operated like the reference process and the reductant cannot be fully utilized.

Fig. 5 also shows that Φ^{TC} reaches higher levels for HTFT than for LTFT and Φ^{Th} vice versa, meaning that in a redox cycle coupled to HTFT, less redox material has to be reduced *via* the energy intense thermal reduction and more of the material is reduced in the less energy intense thermochemical reduction. This effect follows from the higher share of short chained hydrocarbons suitable as reductant in the HTFT product compared to the LTFT product.

3.2. Energy assessment

As mentioned above, optimization of the system is beyond the scope of this study. However, to give an impression of the impact that our novel approach has on the energy efficiency, we select two cases, one for increased δ_{red} and one for decreased T_{red} and compare the energy demand of their reduction steps to that of the reference case. Table 3 contains parameters for the reduction reactors in the two cases and the resulting Φ^{Th} and Φ^{TC} that can be achieved for LTFT and HTFT, respectively. All other parameters are the same as in the reference case, given in Table 2.

The heat demand of the reduction step is given in Figs. 6 and 7. Herein the heat demand is shown relative to that of the reference case. The heat demand is divided into three parts: $\dot{Q}_{ceria}$, the energy needed to heat up ceria to the reduction temperature, according to Equation (2.29), $\Delta_R\dot{H}_{red}$, the enthalpy of reaction for the actual reduction according to Equations (2.30) and (2.31) and radiation losses $\dot{Q}_{loss}$ through the aperture according to Equation (2.33). Fig. 6 shows the energy demand for three reduction reactors that create the same number of vacancies, either thermally (ref. case) or thermochemically (high δ_{red} and low T_{red}).

Fig. 6 shows that in the case with increased δ_{red}, the sensible heat for ceria is greatly reduced as it scales with the amount of ceria, which is low if a high δ_{red} is achieved. Also, radiation losses are reduced, since the overall energy demand is lower, while the ideal receiver efficiency stays the same as for the reference case. The energy demand for the reduction-reaction is in a similar order of magnitude as in the reference case, because the same number of oxygen-vacancies is created. It is however slightly reduced, because the exothermal contribution of the gas phase reaction and the fact that $\Delta_R H^{Th}_{red}$ decreases to some extent with increasing δ_{red}. Since the case with reduced T_{red} represents a virtually isothermal operating point, there is no need to heat ceria in-between reduction and oxidation and the sensible heat demand vanishes. The heat of reaction is almost the same as for the reference case and is only slightly reduced by the exothermal gas phase reaction. Radiation losses are significantly lower than in the reference case and also lower than in the case with increased δ_{red}, because of the high receiver efficiency that results from the low reduction temperature. All in all, the energy demand to create a certain number of oxygen-vacancies in the redox material is reduced to 17% and 10%, when only using thermochemical reduction, compared to purely thermal reduction, for the "high δ_{red}" and "low T_{red}" case of Table 3, respectively.

When recycling gaseous FT products as a reductant, not all reactors are operated with the reductant, but in some reactors the reduction is

Table 3
Parameters for energy assessment.

Case	δ_{red}	T_{red}	p_{red}	$\frac{\dot{n}_{CH_4}}{\dot{n}_{ceria}}$	Φ^{Th}		Φ^{TC}	
					HTFT	LTFT	HTFT	LTFT
High δ_{red}	0.285	1791 K	10^{-3} bar	0.25	0.371	0.755	0.176	0.069
Low T_{red}	0.025	1070 K	10^{-3} bar	0.0167	0.371	0.755	0.190	0.074

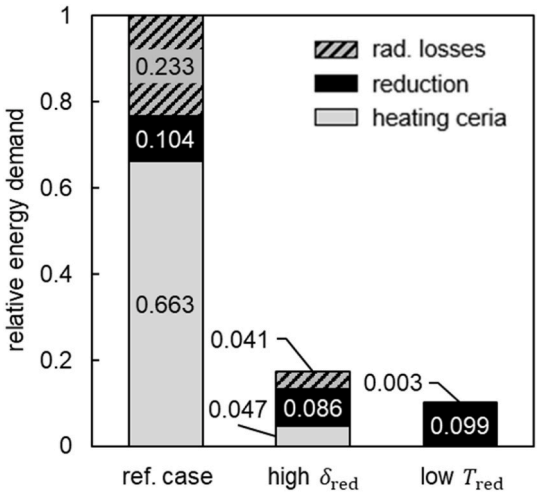

Fig. 6. Relative energy demand of thermal and thermochemical reduction step, if the same number of oxygen vacancies is created.

purely thermal, equal to the reference case. Therefore, the overall heat demand of the reduction is composed of a heat demand for thermal and one for thermochemical reduction, scaling with Φ^{Th} and Φ^{TC}, respectively. Fig. 7 (a) shows results for a process with HTFT with $\alpha = 0.70$, while results for a process including LTFT with $\alpha = 0.84$ are depicted in Fig. 7 (b).

In the reference case, the short-chained hydrocarbons are wasted. Recycling these hydrocarbons reduces the necessary feed stream, according to Equation (2.10), by a factor of $1 - \varphi$ to 53% (HTFT) or 82% (LTFT) of the value for the reference case. The redox cycle and hence the thermal reduction step and its energy demand can be scaled down accordingly. In addition, performing part of the reduction thermochemically scales down the thermal reduction further ($\Phi^{Th} < 1 - \varphi$). Utilizing the reductant significantly reduces the heat demand of the reduction step in both approaches, i.e. increased δ_{red} and decreased T_{red}. Especially when coupling the thermochemical redox cycle to HTFT, as shown in Fig. 7 (a), the energy demand is drastically lower than in the reference case. Here, the total heat demand for the reduction, relative to the reference case, is approximately 40% for the case with high δ_{red} and 39% for the case with low T_{red}. For a thermochemical cycle, which is followed by LTFT, the heat demand is decreased to approximately 77% or 76% of the energy demand of the reference case. Even though this is still a substantial improvement, the effect is considerably less distinct than for HTFT. Reason for that is the different product distribution of the

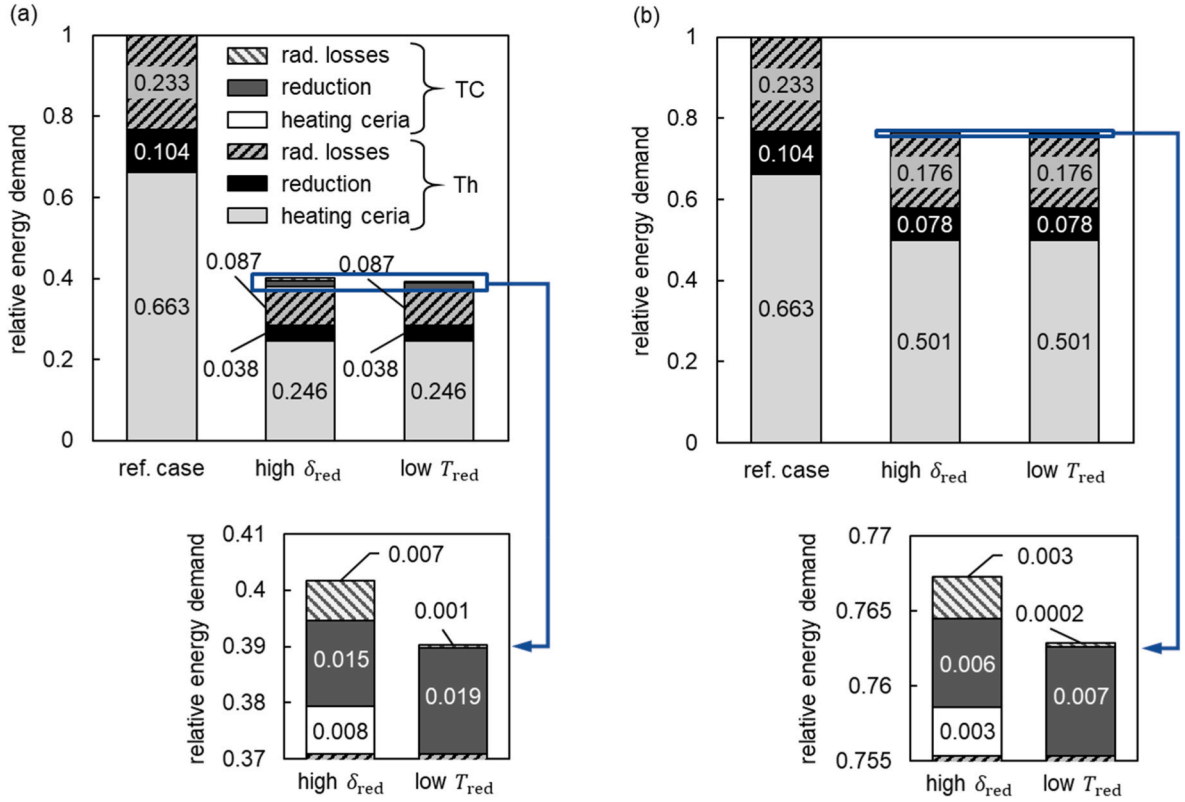

Fig. 7. Relative energy demand of reduction step of novel approach containing both thermal (Th) and thermochemical (TC) reduction, compared to the reference case for different operational modes for (a) HTFT with $\alpha = 0.70$ and (b) LTFT with $\alpha = 0.84$. The magnified areas show the energy contributions for the thermochemical reduction, which are minor compared to the thermal reduction.

two FT modes. As mentioned above, in HTFT a larger portion of the product consists of volatile hydrocarbons that can be used as reductant compared to LTFT. Hence, Φ^{TC} is higher and Φ^{Th} is lower in that case, meaning more syngas can be produced under the beneficial conditions of the novel approach and less of the energy intense thermal reduction is needed.

3.3. Syngas composition

The selectivity of the methane conversion towards CO and H_2 affects the plant design. CO_2 and H_2O in the syngas don't necessarily reduce the syngas yield, because they can be recycled to the oxidation reactor where they are converted to CO and H_2. However, this might require large recycle streams and/or gas separation steps. Fig. 8 (a) shows the product composition of the thermochemical reduction as a function of T_{red}. High temperatures in the reaction of methane with oxygen (Reaction (2.25)) favour the formation of H_2 and CO over H_2O and CO_2, while the latter are dominant at lower temperatures [67]. However, a surplus of oxygen shifts the product composition towards the combustion products H_2O and CO_2. Therefore, in the overall reduction reaction of ceria with methane (Reaction (1.3) with $N = 1$), high temperatures can favour the conversion of methane to H_2O and CO_2 as more oxygen is released from ceria, which can be seen in Fig. 8 (a). The grey vertical line represents the "low T_{red}" case from Table 3. This point of operation yields a product composition of 62% H_2, 31% CO, 4.4% H_2O and 2.4% CO_2.

Fig. 8 (b) shows the product composition of the thermochemical reduction as a function of δ_{red} and the grey vertical line represents the "high δ_{red}" case of Table 3, which was assessed in Fig. 7. For a given temperature, high δ_{red}-values are achieved at lower oxygen partial pressure. Therefore, high oxygen concentrations and consequently a shift to full combustion products are present at low values of δ_{red}. The aforementioned "high δ_{red}" case leads to a similar product composition as the "low T_{red}" case of 63% H_2, 33% CO, 3.6% H_2O and 0.5% CO_2. Even higher values of δ_{red} are, according to data presented in Ref. [66], hardly possible as such strong degrees of reduction would result in an undesired phase change of ceria.

4. Conclusion

A novel approach for solar fuel production *via* a ceria based redox cycle and Fischer-Tropsch synthesis was proposed. Recycling of C_1–C_4 FT by-products and their utilization as a reductant to perform thermochemical reduction of ceria was shown to decrease the energy demand of a reduction reactor compared to a thermal reduction step. Simulations in *Aspen Custom Modeler* and calculations in *Python* were conducted, from which the following findings were obtained.

1. By using by-products in a reactor, the reduction extent δ can be increased drastically compared to purely thermal redox cycles.
2. Alternatively, the reduction of ceria can be operated at significantly lower temperature than in a purely thermal reduction step. A combination of somewhat increased δ and reduced T_{red} seems feasible as well.
3. High δ-values and low temperatures increase the product purity in the thermochemical reduction, i.e. less combustion products are produced and the selectivity is shifted to H_2 and CO.
4. Only part of the total ceria mass used in the process can be reduced thermochemically. Spreading the reductant over a larger amount of ceria does not reduce the amount of ceria that has to be reduced thermally as in this case more H_2O and CO_2 are produced and have to be converted to H_2 and CO in the oxidation step, for which additional oxygen-vacancies are needed.
5. The proposed concept can enhance the efficiency of the reduction step substantially. For the investigated points of operation, the energy demand for the reduction is decreased by up to 61%, when coupled to HTFT and by up to 24%, when coupled to LTFT for operation at 10^{-3} bar.
6. The thermochemical reduction can be performed at higher pressures than the thermal reduction, so that the energy demand for compression of syngas for the FT synthesis and operation of vacuum pumps in the receiver reactor can be decreased.

Our investigation focused on the performance of the reduction step. Potential future work could comprise a comprehensive system analysis, including a comparison to other approaches of recycling C_1–C_4 FT products, such as steam reforming. We assumed that methane can be used as a representative of C_1–C_4 alkanes and incomplete syngas conversion in the Fischer-Tropsch process was not part of the analysis. A more thorough investigation using a mixture of those alkanes and unreacted syngas as reductant might give further insights into the process in the future. Optimization with respect to overall system efficiency as well as more sophisticated modes of operation, including strategies for irradiation of the receiver array and buffering of by-products could reveal the full potential of the concept.

CRediT authorship contribution statement

Philipp Holzemer-Zerhusen: Writing – review & editing, Writing – original draft, Visualization, Validation, Methodology, Investigation,

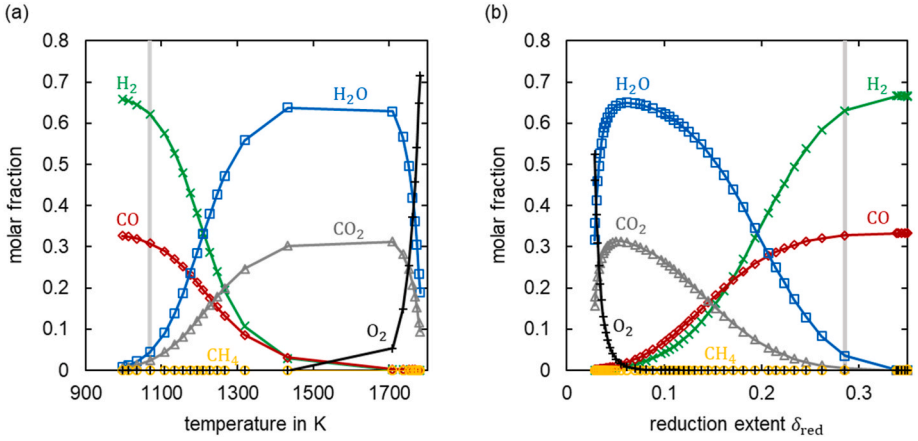

Fig. 8. Syngas composition of the thermochemical reduction. Mole fractions are shown as a function of (a) the reduction temperature and (b) the oxygen non-stoichiometry δ_{red}. For both graphs the pressure is $p_{red} = 10^{-3}$ bar, in (a) $\delta_{red} = 0.025$ and in (b) $T_{red} = 1791$ K. The exemplary points of operation discussed in Fig. 7 are highlighted by vertical lines.

Conceptualization. **Andreas Rosenstiel:** Writing – review & editing, Writing – original draft, Methodology, Investigation, Conceptualization. **Stefan Brendelberger:** Writing – review & editing, Methodology, Formal analysis, Conceptualization. **Martin Roeb:** Writing – review & editing, Investigation, Formal analysis, Conceptualization. **Christian Sattler:** Writing – review & editing, Supervision, Methodology, Conceptualization.

Declaration of competing interest

The authors declare the following financial interests/personal relationships which may be considered as potential competing interests: A patent application was filed related to this work.

Acknowledgements

This work has received financial support through basic funding from DLR within the projects SOLINT and NeoFuels. The authors would like to thank Dr. Nicole Knoblauch for valuable discussions.

References

[1] Fischer F, Tropsch H. Über die Herstellung synthetischer Ölgemische (Synthol) durch Aufbau aus Kohlenoxyd und Wasserstoff. Brennst. Chem 1923;4:276–85.
[2] Zoller S, et al. *A solar tower fuel plant for the thermochemical production of kerosene from H_2O and CO_2*. Joule 2022;6(7):1606–16.
[3] Singh A, et al. Design of a pilot scale directly irradiated, high temperature, and low pressure moving particle cavity chamber for metal oxide reduction. Sol Energy 2017;157:365–76.
[4] Chueh WC, Haile SM. *A thermochemical study of ceria: exploiting an old material for new modes of energy conversion and CO_2 mitigation*. Phil Trans Math Phys Eng Sci 2010;368(1923):3269–94.
[5] Bulfin B, et al. Oxidation and reduction reaction kinetics of mixed cerium zirconium oxides. J Phys Chem C 2016;120(4):2027–35.
[6] Panlener RJ, Blumenthal RN, Garnier JE. A thermodynamic study of nonstoichiometric cerium dioxide. J Phys Chem Solid 1975;36(11):1213–22.
[7] Mogensen M, Sammes NM, Tompsett GA. Physical, chemical and electrochemical properties of pure and doped ceria. Solid State Ionics 2000;129(1–4):63–94.
[8] Marxer D, et al. *Solar thermochemical splitting of CO_2 into separate streams of CO and O_2 with high selectivity, stability, conversion, and efficiency*. Energy Environ Sci 2017;10:1142–9.
[9] Bulfin B, et al. *Analytical Model of CeO_2 Oxidation and reduction*. J Phys Chem C 2013;117(46):24129–37.
[10] Grobbel J, et al. Heat transfer in a directly irradiated ceria particle bed under vacuum conditions. Sol Energy 2017;158:737–45.
[11] Knoblauch N, et al. Chemical expansion of La3+ and Yb3+ incorporated Zr-doped ceria ceramics for concentrated solar energy-driven thermochemical production of fuels. Solid State Ionics 2024;405:116451.
[12] Lee K, et al. Strategic co-doping of ceria for improved oxidation kinetics in solar thermochemical fuel production. Mater Today Energy 2023;35:101321.
[13] Liu X, et al. *Ca- and Ga-doped $LaMnO_3$ for solar thermochemical CO_2 Splitting with high fuel Yield and cycle stability*. ACS Appl Energy Mater 2021;4(9):9000–12.
[14] McDaniel AH, et al. *Sr- and Mn-doped $LaAlO3-\delta$ for solar thermochemical H_2 and CO production*. Energy Environ Sci 2013;6(8):2424–8.
[15] Scheffe JR, Weibel D, Steinfeld A. *Lanthanum–strontium–manganese Perovskites as redox Materials for solar thermochemical Splitting of H_2O and CO_2*. Energy Fuels 2013;27(8):4250–7.
[16] Brendelberger S, et al. Counter flow sweep gas demand for the ceria redox cycle. Sol Energy 2015;122:1011–22.
[17] Warren KJ, et al. Theoretical and experimental investigation of solar methane reforming through the nonstoichiometric ceria redox cycle. Energy Technol 2017;5(11):2138–49.
[18] Furler P, et al. *Thermochemical CO_2 splitting via redox cycling of ceria reticulated foam structures with dual-scale porosities*. Phys Chem Chem Phys 2014;16(22):10503–11.
[19] Chueh WC, et al. High-flux solar-driven thermochemical dissociation of CO_2 and H_2O using nonstoichiometric ceria. Science 2010;330:1797–801.
[20] Abanades S, et al. Investigation of reactive cerium-based oxides for H_2 production by thermochemical two-step water-splitting. J Mater Sci 2010;45(15):4163–73.
[21] Ermanoski I, Siegel NP, Stechel EB. A new reactor concept for efficient solar-thermochemical fuel production. J Sol Energy Eng 2013;135(3):031002.
[22] Venstrom LJ, et al. *Efficient Splitting of CO_2 in an isothermal redox cycle Based on ceria*. Energy Fuels 2014;28:2732–42.
[23] Li S, et al. Thermodynamic analyses of fuel production via solar-driven non-stoichiometric metal oxide redox cycling. Part 1. Revisiting flow and equilibrium assumptions. Energy Fuels 2018;32(10):10838–47.
[24] Li S, et al. Thermodynamic analyses of fuel production via solar-driven non-stoichiometric metal oxide redox cycling. Part 2. Impact of solid–gas flow configurations and active material composition on system-level efficiency. Energy Fuels 2018;32(10):10848–63.
[25] Brendelberger S, et al. Vacuum pumping options for application in solar thermochemical redox cycles – assessment of mechanical-, jet- and thermochemical pumping systems. Sol Energy 2017;141:91–102.
[26] Brendelberger S, et al. Demonstration of thermochemical oxygen pumping for atmosphere control in reduction reactions. Sol Energy 2018;170:273–9.
[27] Brendelberger S, et al. Thermochemical oxygen pumping for improved hydrogen production in solar redox cycles. Int J Hydrogen Energy 2019.
[28] Pein M, et al. Redox thermochemistry of Ca-Mn-based perovskites for oxygen atmosphere control in solar-thermochemical processes. Sol Energy 2020;198:612–22.
[29] Ermanoski I, Stechel EB. Thermally-driven adsorption/desorption cycle for oxygen pumping in thermochemical fuel production. Sol Energy 2020;198:578–85.
[30] Xu M, et al. Oxygen pumping characteristics of YBaCo4O7+δ for solar thermochemical cycles. Chem Eng J 2020;389:124026.
[31] Xu M, et al. Sorbent-based oxygen separation with YBC114 for energy storage systems. Chem Eng J 2022;435:134884.
[32] Ehrhart BD, et al. System efficiency for two-step metal oxide solar thermochemical hydrogen production – Part 3: various methods for achieving low oxygen partial pressures in the reduction reaction. Int J Hydrogen Energy 2016;41(44):19904–14.
[33] Krenzke PT, Fosheim JR, Davidson JH. Solar fuels via chemical-looping reforming. Sol Energy 2017;156:48–72.
[34] Krenzke PT, et al. Synthesis gas production via the solar partial oxidation of methane-ceria redox cycle: conversion, selectivity, and efficiency. Int J Hydrogen Energy 2016;41(30):12799–811.
[35] Sheu EJ, Ghoniem AF. Redox reforming based, integrated solar-natural gas plants: reforming and thermodynamic cycle efficiency. Int J Hydrogen Energy 2014;39(27):14817–33.
[36] Sheu EJ, Mokheimer EM, Ghoniem AF. Dry redox reforming hybrid power cycle: performance analysis and comparison to steam redox reforming. Int J Hydrogen Energy 2015;40(7):2939–49.
[37] He F, et al. A hybrid solar-redox scheme for liquid fuel and hydrogen coproduction. Energy Environ Sci 2014;7(6):2033–42.
[38] Welte M, et al. Combined Ceria reduction and methane reforming in a solar-driven particle-transport reactor. Ind Eng Chem Res 2017;56(37):10300–8.
[39] Holzemer-Zerhusen P, et al. Efficiency assessment of solar redox reforming in comparison to conventional reforming. Int J Hydrogen Energy 2020;45(7):4137–51.
[40] Bulfin B, et al. Thermodynamic comparison of solar methane reforming via catalytic and redox cycle routes. Sol Energy 2021;215:169–78.
[41] Zuber M, et al. Methane dry reforming via a ceria-based redox cycle in a concentrating solar tower. Sustain Energy Fuels 2023;7(8):1804–17.
[42] Schäppi R, et al. Drop-in fuels from sunlight and air. Nature 2022;601(7891):63–8.
[43] Nguyen VN, Blum L. *Syngas and Synfuels from H_2O and CO_2: current status*. Chem Ing Tech 2015;87(4):354–75.
[44] Marxer DA, et al. *Demonstration of the entire production chain to renewable kerosene via solar-thermochemical splitting of H_2O and CO_2*. Energy Fuels 2015.
[45] Lange M, et al. T–S diagram efficiency analysis of two-step thermochemical cycles for solar water splitting under various process conditions. Energy 2014;67(0):298–308.
[46] Koepf E, et al. Liquid fuels from concentrated sunlight: an overview on development and integration of a 50 kW solar thermochemical reactor and high concentration solar field for the SUN-to-LIQUID project. In: SolarPACES; 2018. Morocco.
[47] Brendelberger S, et al. Performance analysis of operational strategies for monolithic receiver-reactor arrays in solar thermochemical hydrogen production plants 2020;45(49):26104–16.
[48] Grobbel J, et al. Operation optimization of an array of receiver-reactors for solar fuel production. AIP Conf Proc 2022;2445(1):130004.
[49] Oberkirsch L, et al. Controlling a solar receiver with multiple thermochemical reactors for hydrogen production by an LSTM neural network based cascade controller. Sol Energy 2022;243:483–93.
[50] Diver RB, et al. Solar thermochemical water-splitting ferrite-cycle heat engines. J Sol Energy Eng 2008;130(4):41001–8.
[51] Lapp J, Davidson JH, Lipiński W. Heat transfer analysis of a solid-solid heat recuperation system for solar-driven nonstoichiometric redox cycles. J Sol Energy Eng 2013;135(3):031004.
[52] Felinks J, et al. Heat recovery concept for thermochemical processes using a solid heat transfer medium. Appl Therm Eng 2014;73(1):1006–13.
[53] Siegrist S, et al. Moving brick receiver–reactor: a solar thermochemical reactor and process design with a solid–solid heat exchanger and on-demand production of hydrogen and/or carbon monoxide. J Sol Energy Eng 2019;141(2).
[54] Falter CP, Sizmann A, Pitz-Paal R. Modular reactor model for the solar thermochemical production of syngas incorporating counter-flow solid heat exchange. Sol Energy 2015;122:1296–308.
[55] Brendelberger S, et al. Study of a new receiver-reactor cavity system with multiple mobile redox units for solar thermochemical water splitting. Sol Energy 2022;235:118–28.
[56] Patankar AS, et al. A reactor train system for efficient solar thermochemical fuel Production1. J Sol Energy Eng 2022;144(6).
[57] Holzemer-Zerhusen P, et al. Oxygen crossover in solid–solid heat exchangers for solar water and carbon dioxide splitting: a thermodynamic analysis. J Energy Resour Technol 2020;143(7).
[58] Klerk Ad. Fischer-Tropsch refining. Weinheim: Wiley-VCH-Verl; 2011.
[59] Murzin D. Chemical reaction technology. Berlin/Boston: De Gruyter; 2015.
[60] Coonradt HL, Garwood WE. Mechanism of hydrocracking. Reactions of paraffins and olefins. Ind Eng Chem Process Des Dev 1964;3(1):38–45.

[61] Falter C, et al. SUN-to-LIQUID. Public report D1.7: life-cycle analysis, social benefits and environmental impact analysis. 2016.
[62] Fan L, Li F, Ramkumar S. Utilization of chemical looping strategy in coal gasification processes. Particuology 2008;6(3):131–42.
[63] Li F, Fan L-S. Clean coal conversion processes – progress and challenges. Energy Environ Sci 2008;1(2):248–67.
[64] Adelung S, Maier S, Dietrich R-U. Impact of the reverse water-gas shift operating conditions on the Power-to-Liquid process efficiency. Sustain Energy Technol Assessments 2021;43:100897.
[65] Bulfin B, et al. Thermodynamics of CeO2 thermochemical fuel production. Energy Fuels 2015;29(2):1001–9.
[66] Zinkevich M, Djurovic D, Aldinger F. Thermodynamic modelling of the cerium–oxygen system. Solid State Ionics 2006;177(11–12):989–1001.
[67] Krenzke PT, Davidson JH. Thermodynamic analysis of syngas production via the solar thermochemical cerium oxide redox cycle with methane-driven reduction. Energy Fuels 2014;28(6):4088–95.